ISSN 0016-8521, Geotectonics, 2019, Vol. 53, No. 1, pp. 110–124. © Pleiades Publishing, Inc., 2019.

Two Types of Plagiogranite from Mesozoic Ashin Ophiolite (Central Iran): a Mark of Tectonic Setting Change from Jurassic to Cretaceous[1]

G. Torabi[a, *], T. Morishita[b], and S. Arai[c]

[a] *University of Isfahan, Department of Geology, Isfahan, P.C. 8174673441 Iran*

[b] *Kanazawa University-School of Natural System, College of Science and Engineering, Kanazawa, P.C. 920–1192 Japan*

[c] *Kanazawa University-Institute of Liberal Arts and Science, Kanazawa, 920–1192 Japan*

**e-mail: Torabighodrat@sci.ui.ac.ir*

Received November 17, 2017; Revised April 13, 2018; Accepted September 25, 2018

Abstract—The Ashin ophiolite is situated in the western part of Central Iran and presents two stages of Jurassic and Cretaceous spreading. The Ashin ophiolite represents fragments of the Neo-Tethys oceanic lithosphere. Plagiogranite intrusions of this ophiolite have good exposures. Plagiogranites of Cretaceous are more fresh than the metamorphosed samples of Jurassic. The main minerals of plagiogranites from the Ashin ophiolite are plagioclase, quartz and amphibole. Plagiogranites of the Jurassic have tholeitic nature with higher amounts of amphibole, $Fe_2O_3^*$, TiO_2, Co and lower values of Mg#, Th and Sr than the Cretaceous calc-alkaline plagiogranites. The chondrite-normalized REE patterns of these plagiogranites are characterized by higher values of REEs and negative Eu anomalies for the Jurassic samples and low values of REEs and positive Eu anomalies for the Cretaceous ones. Very low values of HREEs in the Cretaceous plagiogranites indicates a non-peridotitic source rock. We suggest that the Jurassic plagiogranites are formed by fractional crystallization of a low-K tholeitic magma; and the adakitic Cretaceous plagiogranites are formed by partial melting of an amphibolite in the subducting slab. Geochemical criteria of the Ashin plagiogranites indicate changing the Ashin ophiolite tectonic setting from a mid-ocean ridge system in the Jurassic to a supra-subduction zone in the Cretaceous.

Keywords: Neo-Tethys, ophiolite, plagiogranite, Jurassic, Cretaceous, Ashin, Central Iran

DOI: 10.1134/S0016852119010084

INTRODUCTION

Plagiogranites are leucocratic igneous rocks usually found as irregular bodies in association with ophiolitic cumulate gabbros and sheeted dykes. These acidic rocks are considered as differentiates of subalkaline tholeitic basalts [4], or partial melting products of a hydrothermally altered oceanic crust [2, 13]. The first mechanism can form most of the range of the ophiolitic plagiogranites [11]. They essentially are composed of plagioclase, quartz and accessory ferromagnesian minerals (e.g. amphibole). Coleman and Peterman [5] suggested using of "oceanic plagiogranite" term for leucocratic rocks of ophiolites. Plagiogranites are found in all tectonic subgroups (normal oceanic ridges, anomalous ocean ridges, back-arc basin and supra-subduction zone) [28–30].

Presence of Paleo-Tethys and Neo-Tethys related ophiolitic suits in Iran point to the spreading and closure of oceanic crusts during Paleozoic and Mesozoic eras [26, 34, 35, 38–41]. Plagiogranites are one of the important rock units of Iranian ophioites. In this article, the plagiogranites of the Ashin ophiolite (west of the Anarak area, Central Iran) will be discussed in petrological and chemical points of views. It hoped that this research will be useful in understanding the nature of ophiolitic rocks, as well as the geological history and geodynamical evolution of Iranian No-Tehys related ophiolites.

GEOLOGICAL SETTING

Ophiolite complexes of Iran are part of Middle East Tethyan ophiolite belts. They link to other Asian ophiolites, such as Pakistan in the east, or ophiolites in the Mediterranean region, such as Turkish, Troodos, and east Europe in the west [38]. Iranian ophiolites geographically can be classified into four groups (Fig. 1):

(1) ophiolites along the northern Alborz mountain range, Northern Iran, including the Rasht ophiolites;

[1] The article is published in the original.

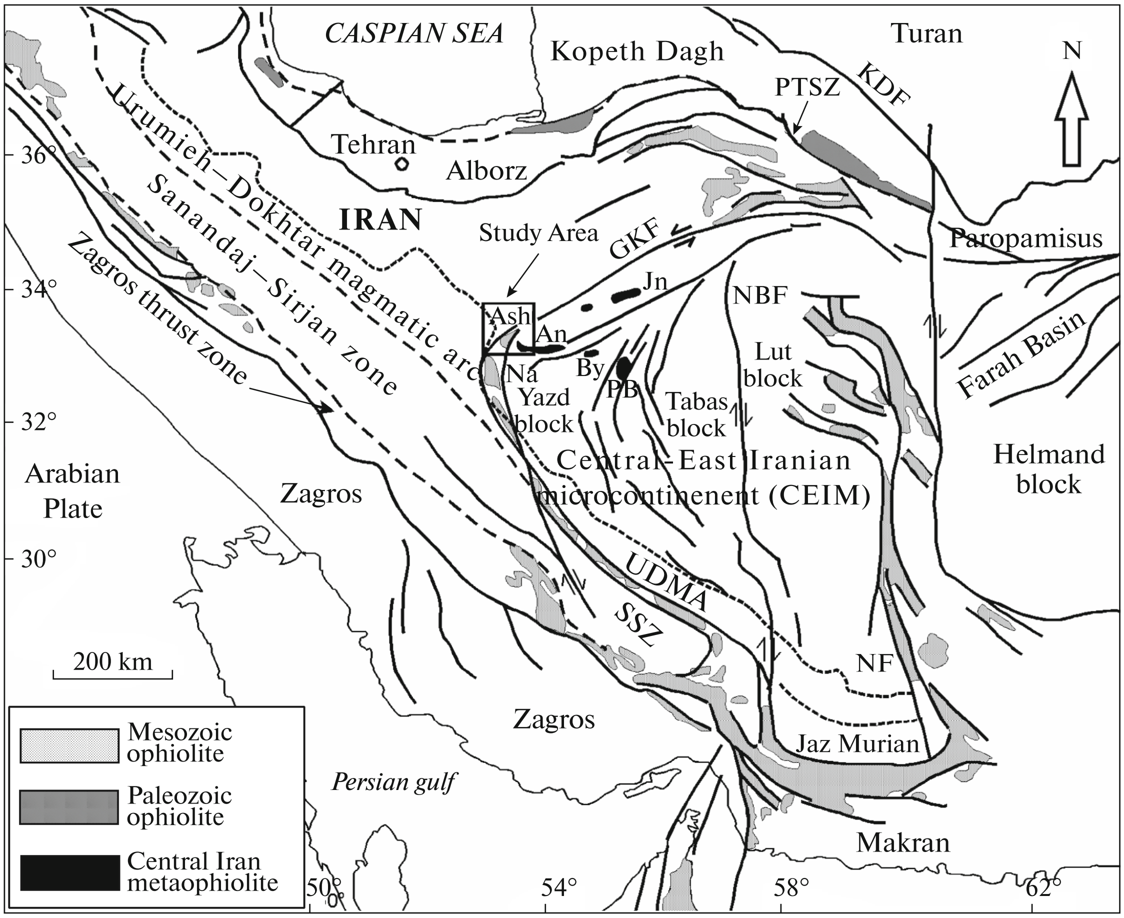

Fig. 1. Main structural units of Iran and location of the Ashin area. GKF—Great Kavir fault, NBF—Naiband fault, NF—Nehbandan fault, SSZ—Sanandaj–Sirjan zone, PTSZ—Paleo-Tethys suture zone, KDF—Kopeth Dagh fault, UDMA—Urumieh–Dokhtar magmatic arc. Ash, An, Jn, By, and PB are Ashin, Anarak, Jandaq, Bayazeh, and Posht-e-Badam ophiolites, respectively.

(2) ophiolites that crop out in the western part of the CEIM, including the Jandaq, Posht-e-Badam, Bayazeh, and Anarak ophiolites;

(3) ophiolites of the Zagros thrust zone including the Neyriz and Kermanshah ophiolites which are regareded as the extension of the Oman ophiolites;

(4) ophiolites and colored melanges that surround the CEIM (Central–East Iranian Microcontinent), e.g. Naein and Ashin ophiolites.

The first and the second group of Iran ophiolites belong to the Paleozoic and are considered as the remnants of the Paleo-Tethys. On the other hand, the third and the fourth groups present the Mesozoic age and are remnants of the Neo-Tethys ocean.

The Ashin area is situated in the western part of the CEIM (Fig. 1), and at the southern margin of Great Kavir with highly deserted climatic and geographical conditions. The Ashin ophiolite mélange is situated in western part of the CEIM, west of the Anarak area, and Ashin and Zavar farms (Figs. 1, 2). It is considered as a remnant of the Neo-Tethys ocean [35]. Geological field investigations suggest that the Ashin ophiolite and associated sedimentary and metamorphic bodies have been emplaced into their present crustal level during the Paleocene to Early Eocene.

The Ashin ophiolitic massif is consists of mantle and serpentinized mantle peridotite, chromitite, gabbro, pyroxenite, dike, pillow lava, plagiogranite, listwaenite, rodingite and strongly foliated metamorphic rocks (foliated amphibolitic dikes, amphibolite, skarn, banded meta-cherts and succession of schist and marble). It has been covered by the Cretaceous limestone. The serpentinite and serpentinized ultramafic rocks of mantle origin are the matrix for the other mentioned units. All of the rock units mentioned above intermixed forming a colored ophiolitic mélange. Predominant rock type of mantle peridotites is harzburgite [35].

The Ashin ophiolite plagiogranites usually occur as stocks and small dykes and veinlets in the upper part of the ophiolite sequence (Fig. 3). Plagiogranites occur as intrusives within the gabbro and dyke complex. Sometimes, they also intrude the mantle peridotite units of the Ashin ophiolite. The studied dikes exhibit sharp boundaries in contact with the surrounding per-

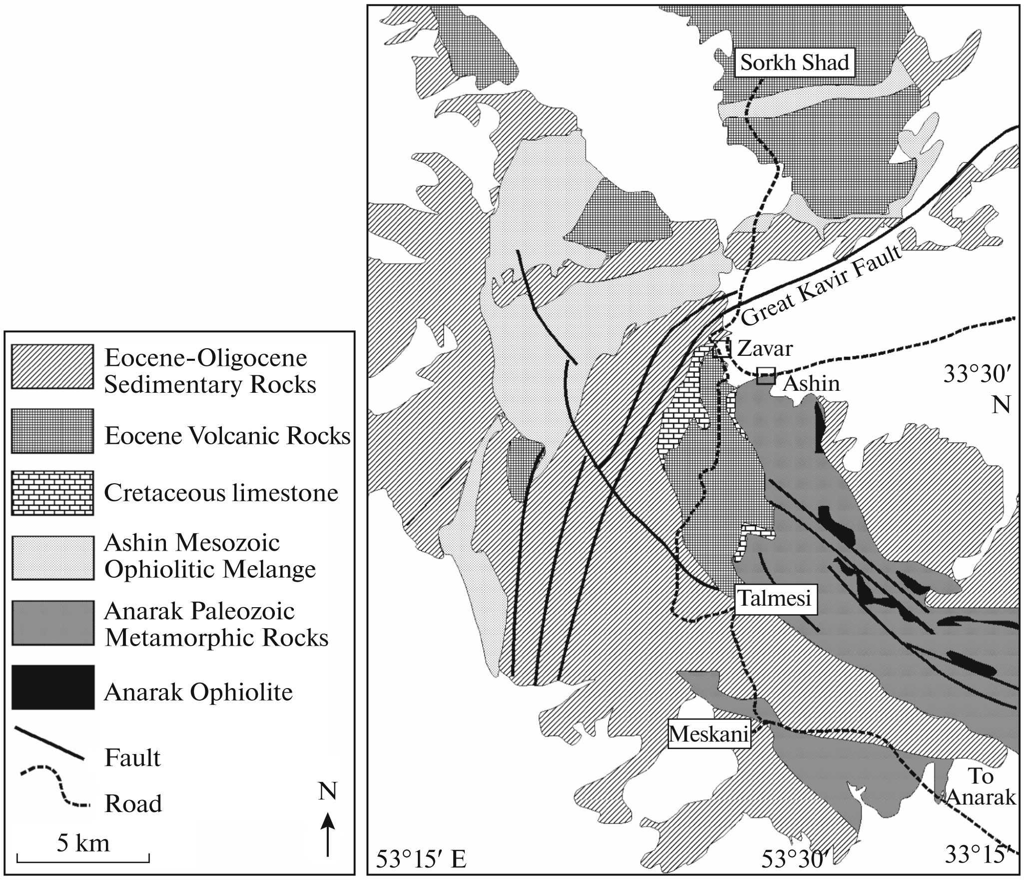

Fig. 2. Simplified geological map of the Ashin area (Isfahan province, Central Iran).

idotites. The thickness of the dikes and veinlets are commonly in the range of a few centimeters to about two meters. A limited form of plagiogranitic dike swarm found in the central part of the Ashin ophiolite. In this exposure, the plagiogranite dike swarm cross cuts the basic sheeted dyke and pillow lava. K-Ar dating of plagiogranites from the Ashin ophiolite yielded two distinct ages of 98 (Lower part of the Upper Cretaceous) and 188 (Lower Jurassic) Ma [32]. The older plagiogranites generally exhibit cataclastic deformation.

ANALYTICAL TECHNIQUES

Mineral chemical compositions were measured at Kanazawa University (Kanazawa, Japan) using a wavelength dispersive electron probe microanalyzer (EPMA) (JEOL JXA-8800R), with 20 kV accelerating potential, 20 nA beam current with 3-μm probe beam diameter (Tables 1, 2). The standard ZAF correction procedures was used for data correction. Natural minerals and synthetic glasses of known composition were used as standards. The Fe^{3+} contents of minerals were calculated by assuming mineral stoichiometry. Mg# of minerals calculated as $Mg/(Mg + Fe^{2+})$.

Whole-rock major and trace element concentrations were determined by Neutron Activation Analysis (NAA) in the Isfahan Activation Center. The quality assurance of the NAA results was evaluated by analyzing certified Standard Reference Materials (SRM) prepared by the Canadian Certified Reference Material Project (CCRMP), Republic of South Africa Bureau of Standards (SACCRM), and China National Analysis Center, as well as repeating the analyses. Two whole rock (Ashj14 and Ashc23) major and trace element analyses were determined by Inductively Coupled Plasma Mass Spectrometry (ICP-MS) in the Nancy University (France) (Table 3). The FeO and Fe_2O_3 concentrations of the analyzed whole rock samples are recalculated from $Fe_2O_3^*$ using the recommended ratios of [25]. Mineral abbreviations are from [43].

PETROGRAPHY AND MINERAL CHEMISTRY

High value of plagioclase is evident in the petrography of the studied plagiogranites. In the Jurassic plagiogranites, the main minerals are plagioclase and quartz (Fig. 4). Minor minerals are amphibole, zircon, apatite and ilmenite. Graphic intergrowths of

Fig. 3. Field photos of the Cretaceous (a, b), and Jurassic (c, d) plagiogranites in the Ashin ophiolite and associated rocks.

plagioclase and quartz suggests simultaneous crystallization of these minerals in the eutectic point. Mineralogical assemblage of the Jurassic plagiogranites indicate that they have undergone a wide spread of hydrothermal alteration. All of the Jurassic samples contain secondary minerals of chlorite, epidote and albite. These minerals have developed at the expense of amphibole and primary igneous plagioclase. Even though of alteration effects in these samples, the modal consistency and preservation of most of primary igneous textures, reveal their primary igneous nature. All amphiboles in the studied samples represent calcic nature (Fig. 5). Amphiboles of the Jurassic samples are magnesio-hornblende, actinolitic hornblende and actinolite in composition (Fig. 5c) with Mg# ranging from 0.52 to 0.67 (Table 1). All plagioclases in the Jurassic samples are albite in composition (Fig. 5a). According to the alteration, all primary plagioclases are changed to albite. Chlorites are ripodolite in composition with Mg# ranging from 0.45 to 0.48. The average value of pistacite number (Ps# = $[Fe^{3+}/(Fe^{3+} + Al)] \times 100$) of epidotes is 27.4%.

Under the microscope the Ashin Cretaceous plagiogranites consist essentially of plagioclase, and quartz (Fig. 4). Amphibole, zircon, apatite and rutile are as minor minerals. Plagioclase and quartz grains are found as subhedral to anhedral minerals with medium grain size (0.5 to 1 mm). The main texture is granular, and zoning of plagioclase is evident. The Cretaceous plagiogranites are more fresh than the Jurassic ones. In some Cretaceous samples, albite and sericite are present as the alteration products of plagiocalse. Lack of metamorphic fabrics (e.g. foliation or lineation) demonstrates that they underwent a low temperature static hydrothermal event. Amphiboles of Cretaceous samples have calcic nature and are tremolite in composition (Table 2) and plagioclases have oligoclase and albite chemistry. FeO* content of rutiles is 0.37 to ~ 1 wt %.

The microprobe analyses of plagioclase in the Cretaceous plagiogranites confirm the normal compositional zoning of this mineral (Ab content of 76% in the core increase to 93% in the rim) (Table 2). A systematic decrease in CaO values and increase in Na_2O amounts from core to rim is evident. Such compositional trends reflect interaction of crystal and liquid during magma crystallization. Normal zoning of chemical composition in plagioclases and granophyric intergrowths (graphic and vermicular textures) indicate that these rocks are the product of igneous processes.

Table 1. Chemical composition of minerals (wt%) in the Jurassic plagiogranites from Ashin ophiolite (Central Iran) and their calculated structural formula

Sample	**270**	**270**	**270**	**270**	**270**	**270**	**270**	**270**	**270**	**270**	**270**	**270**	**270**	**270**	**270**	**270**
analysis	**24**	**27**	**30**	**5**		**21**	**23**	**25**	**26**	**28**	**29**	**8**	**31**	**9**	**32**	**33**
age	**Jurassic**	**Jurassic**	**Jurassic**	**Jurassic**	**Jurassic**	**Jurassic**	**Jurassic**	**Jurassic**	**Jurassic**	**Jurassic**	**Jurassic**	**Jurassic**	**Jurassic**	**Jurassic**	**Jurassic**	**Jurassic**
mineral	**Plg**	**Plg**	**Plg**	**Plg**	**Epd**	**Amp**	**Amp**	**Amp**	**Amp**	**Amp**	**Amp**	**Amp**	**Chl**	**Chl**	**Ilm**	**Ilm**
SiO_2	68.76	68.37	68.91	67.56	37.95	52.81	49.28	49.75	49.02	47.76	47.63	48.51	26.61	25.71	0.59	0.03
TiO_2	0.00	0.00	0.00	0.02	0.31	0.40	1.14	0.84	0.94	1.29	1.24	1.04	0.00	0.02	45.89	48.07
Al_2O_3	19.61	19.83	19.73	19.42	22.72	1.56	3.55	3.17	3.65	4.66	4.48	3.32	19.80	19.53	0.04	0.01
Cr_2O_3	0.00	0.00	0.00	0.00	0.01	0.00	0.06	0.01	0.00	0.02	0.00	0.02	0.00	0.02	0.00	0.00
FeO*	0.00	0.11	0.02	0.03	12.09	18.59	19.55	20.93	21.28	20.92	19.38	21.77	27.64	27.59	46.43	45.29
MnO	0.00	0.02	0.02	0.00	0.02	0.48	0.41	0.42	0.46	0.31	0.51	0.53	0.29	0.21	1.89	2.11
MgO	0.00	0.00	0.00	0.00	0.09	12.48	11.21	11.04	10.61	9.73	10.56	10.73	12.69	14.46	0.10	0.10
CaO	0.16	0.59	0.35	0.23	21.44	10.17	9.56	8.88	8.78	9.95	10.16	8.87	0.11	0.11	0.53	0.05
Na_2O	11.93	11.37	11.70	11.29	0.01	0.92	1.94	1.98	2.25	1.97	1.94	1.53	0.01	0.00	0.00	0.00
K_2O	0.05	0.03	0.04	0.23	0.00	0.10	0.40	0.32	0.34	0.48	0.44	0.32	0.07	0.00	0.00	0.00
Total	**100.51**	**100.32**	**100.76**	**98.78**	**94.64**	**97.50**	**97.04**	**97.34**	**97.35**	**97.07**	**96.33**	**96.62**	**87.22**	**87.65**	**95.47**	**95.65**
Oxygen#	8	8	8	8	12.5	23	23	23	23	23	23	23	28	28	3	3
Si	2.990	2.979	2.988	2.988	3.064	7.670	7.299	7.313	7.239	7.178	7.183	7.177	5.700	5.498	0.015	0.001
Ti	0.000	0.000	0.000	0.001	0.019	0.043	0.126	0.093	0.105	0.146	0.140	0.116	0.000	0.003	0.905	0.951
Al	1.004	1.017	1.007	1.012	2.162	0.266	0.619	0.548	0.635	0.824	0.795	0.578	4.997	4.918	0.001	0.000
Cr	0.000	0.000	0.000	0.000	0.000	0.000	0.007	0.001	0.000	0.002	0.000	0.002	0.000	0.003	0.000	0.000
Fe^{3+}	0.000	0.004	0.001	0.001	0.000	0.865	0.853	1.218	1.187	0.656	0.625	1.523	0.000	0.000	0.159	0.097
Fe^{2+}	0.000	0.000	0.000	0.000	0.816	1.393	1.569	1.356	1.441	1.973	1.819	1.171	4.952	4.934	0.859	0.899
Mn	0.000	0.001	0.001	0.000	0.001	0.059	0.051	0.052	0.058	0.040	0.064	0.066	0.053	0.038	0.042	0.047
Mg	0.000	0.000	0.000	0.000	0.011	2.703	2.475	2.419	2.335	2.181	2.373	2.367	4.053	4.610	0.004	0.004
Ca	0.008	0.028	0.016	0.011	1.855	1.583	1.518	1.399	1.389	1.602	1.641	1.406	0.026	0.025	0.015	0.001
Na	1.006	0.961	0.984	0.968	0.002	0.259	0.558	0.563	0.646	0.573	0.566	0.439	0.004	0.000	0.000	0.000
K	0.003	0.002	0.002	0.013	0.000	0.018	0.076	0.060	0.065	0.093	0.085	0.060	0.018	0.000	0.000	0.000
Sum	**5.011**	**4.992**	**4.999**	**4.994**	**7.93**	**14.859**	**15.151**	**15.022**	**15.100**	**15.268**	**15.292**	**14.905**	**19.803**	**20.029**	**2.000**	**2.000**
Ab	98.9	97	98.2	97.6	–	–	–	–	–	–	–	–	–	–	–	–
An	0.8	2.8	1.6	1.1	–	–	–	–	–	–	–	–	–	–	–	–
Or	0.3	0.2	0.2	1.3	–	–	–	–	–	–	–	–	–	–	–	–
Mg#	–	–	–	–	–	0.660	0.612	0.641	0.618	0.525	0.566	0.669	0.45	0.48	–	–

Table 2. Chemical composition of minerals (wt%) in the Cretaceous plagiogranites from Ashin ophiolite (Central Iran) and their calculated structural formula

Sample	**160**	**160**	**160**	**160**	**160**	**160**	**160**	**160**	**160**	**160**	**160**	**160**	**160**	**160**	**160**	**160**	**160**	**160**	**160**	**160**	**160**
analysis	**1(Z1)**	**2(Z2)**	**3(Z3)**	**4**	**7(Z1)**	**8(Z2)**	**9(Z3)**	**10(Z4)**	**11(Z5)**	**12**	**13**	**14**	**15**	**16**	**20**	**6**	**6-1**	**7-1**	**17**	**18**	**19**
age	**Cret.**	**Cret.**	**Cret.**	**Cret.**	**Cret.**	**Cret.**	**Cret.**	**Cret.**	**Cret.**	**Cret.**	**Cret.**	**Cret.**	**Cret.**	**Cret.**	**Cret.**	**Cret.**	**Cret.**	**Cret.**	**Cret.**	**Cret.**	**Cret.**
mineral	**Plg**	**Plg**	**Plg**	**Alt.Plg**	**Plg**	**Plg**	**Plg**	**Plg**	**Plg**	**Amp**	**Amp**	**Amp**	**Amp**	**Amp**	**Amp**	**Amp**	**Amp**	**Amp**	**Rutile**	**Rutile**	**Rutile**
SiO_2	63.60	63.11	66.31	69.78	62.55	63.16	63.31	64.73	65.78	56.15	56.10	56.27	56.44	56.83	56.26	56.31	56.38	57.03	0.08	0.06	0.03
TiO_2	0.03	0.00	0.00	0.02	0.00	0.00	0.01	0.01	0.00	0.30	0.22	0.29	0.27	0.22	0.56	0.34	0.32	0.19	97.87	97.75	98.31
Al_2O_3	22.98	22.90	20.64	19.07	23.44	22.70	22.67	22.10	21.07	1.40	1.29	1.60	1.44	1.19	2.54	1.48	1.27	1.74	0.03	0.05	0.03
Cr_2O_3	0.00	0.00	0.00	0.00	0.00	0.00	0.00	0.00	0.00	0.00	0.00	0.03	0.07	0.00	0.02	0.02	0.00	0.04	0.10	0.08	0.17
FeO*	0.05	0.04	0.08	0.04	0.07	0.03	0.06	0.07	0.02	2.78	2.88	3.62	3.73	3.24	4.13	3.29	3.41	3.52	0.37	0.45	1.04
MnO	0.00	0.00	0.00	0.00	0.01	0.01	0.00	0.00	0.01	0.06	0.04	0.07	0.07	0.06	0.08	0.04	0.03	0.07	0.00	0.01	0.00
MgO	0.00	0.00	0.02	0.02	0.00	0.00	0.00	0.00	0.00	22.49	22.49	22.15	22.25	22.45	21.64	22.79	21.80	21.90	0.00	0.02	0.01
CaO	3.46	3.41	1.16	0.23	4.83	4.15	3.93	3.19	2.06	12.14	12.14	11.86	11.82	12.12	12.23	10.75	12.20	10.66	0.22	0.23	0.01
Na_2O	9.16	9.37	10.67	11.31	8.81	9.13	9.45	9.79	10.49	0.41	0.38	0.42	0.43	0.36	0.50	0.41	0.36	0.06	0.00	0.02	0.00
K_2O	0.21	0.20	0.22	0.09	0.20	0.21	0.21	0.24	0.30	0.01	0.02	0.01	0.01	0.02	0.04	0.03	0.01	0.03	0.00	0.00	0.00
Total	**99.48**	**99.02**	**99.10**	**100.56**	**99.92**	**99.39**	**99.65**	**100.12**	**99.73**	**95.73**	**95.55**	**96.27**	**96.46**	**96.48**	**97.98**	**95.44**	**95.77**	**95.20**	**98.69**	**98.66**	**99.60**
Oxygen#	8	8	8	8	8	8	8	8	8	23	23	23	23	23	23	23	23	23	2	2	2
Si	2.817	2.811	2.932	3.023	2.773	2.808	2.809	2.850	2.901	7.772	7.779	7.742	7.744	7.807	7.661	7.698	7.841	7.812	0.001	0.001	0.000
Ti	0.001	0.000	0.000	0.001	0.000	0.000	0.000	0.000	0.000	0.031	0.023	0.030	0.028	0.023	0.057	0.035	0.033	0.020	0.991	0.989	0.987
Al	1.198	1.201	1.075	0.973	1.224	1.189	1.185	1.146	1.094	0.229	0.211	0.259	0.232	0.193	0.408	0.239	0.207	0.281	0.000	0.001	0.001
Cr	0.000	0.000	0.000	0.000	0.000	0.000	0.000	0.000	0.000	0.000	0.000	0.003	0.008	0.000	0.002	0.002	0.000	0.004	0.001	0.001	0.002
Fe^{3+}	0.002	0.001	0.003	0.001	0.003	0.001	0.002	0.002	0.001	0.321	0.334	0.416	0.429	0.373	0.446	0.376	0.311	0.403	0.000	0.000	0.000
Fe^{2+}	0.000	0.000	0.000	0.000	0.000	0.000	0.000	0.000	0.000	0.000	0.000	0.000	0.000	0.000	0.025	0.000	0.086	0.000	0.005	0.005	0.012
Mn	0.000	0.000	0.000	0.000	0.000	0.000	0.000	0.000	0.000	0.007	0.004	0.008	0.008	0.007	0.010	0.005	0.004	0.008	0.000	0.000	0.000
Mg	0.000	0.000	0.001	0.001	0.000	0.000	0.000	0.000	0.000	4.640	4.650	4.542	4.551	4.598	4.392	4.644	4.519	4.472	0.000	0.000	0.000
Ca	0.164	0.163	0.055	0.011	0.229	0.198	0.187	0.150	0.097	1.800	1.803	1.748	1.738	1.783	1.785	1.574	1.818	1.565	0.003	0.003	0.000
Na	0.787	0.809	0.915	0.950	0.757	0.787	0.813	0.836	0.897	0.109	0.101	0.112	0.115	0.096	0.133	0.109	0.097	0.015	0.000	0.001	0.000
K	0.012	0.011	0.013	0.005	0.011	0.012	0.012	0.013	0.017	0.001	0.003	0.002	0.001	0.003	0.006	0.005	0.002	0.005	0.000	0.000	0.000
Sum	**4.981**	**4.996**	**4.994**	**4.965**	**4.997**	**4.995**	**5.008**	**4.997**	**5.007**	**14.910**	**14.908**	**14.862**	**14.854**	**14.882**	**14.924**	**14.687**	**14.916**	**14.585**	**1.000**	**1.000**	**1.000**
Ab	81.7	82.3	93.1	98.3	75.9	78.9	80.3	83.7	88.7	–	–	–	–	–	–	–	–	–	–	–	–
An	17	16.6	5.6	1.1	23	19.9	18.5	15	9.6	–	–	–	–	–	–	–	–	–	–	–	–
Or	1.2	1.1	1.3	0.5	1.1	1.2	1.2	1.3	1.7	–	–	–	–	–	–	–	–	–	–	–	–
Mg#	–	–	–	–	–	–	–	–	–	1	1	1	1	1	0.994	1	0.981	1	–	–	–

Analyses of zoned plagioclases are from core to rim.

Table 3. Geochemical whole rock compositions of plagiogranites from the Ashin ophiolite (Central Iran)

Sample	Ashj11	Ashj12	Ashj13	Ashj14	Ashj15	Ashj16	AV.	Ashc21	Ashc22	Ashc23	Ashc24	Ashc25	Ashc26	AV.
Age	**Juras.**	**Juras.**	**Juras.**	**Juras.**	**Juras.**	**Juras.**	**Juras.**	**Cret.**	**Cret.**	**Cret.**	**Cret.**	**Cret.**	**Cret.**	**Cret.**
SiO_2	74.56	68.73	67.98	68.31	73.26	69.82	**70.44**	74.03	69.85	72.71	73.14	73.48	71.12	**72.39**
TiO_2	0.32	0.55	0.35	0.55	0.41	0.47	**0.44**	0.1	0.17	0.21	0.22	0.19	0.2	**0.18**
Al_2O_3	12.76	14.21	14.06	14.38	13.18	13.9	**13.75**	14.17	17.31	14.64	14.89	13.96	15.51	**15.08**
$Fe_2O_3^*$	2.43	3.66	5.15	4.87	2.97	4.03	**3.85**	0.27	0.27	0.38	0.4	0.3	0.35	**0.33**
FeO(cal)	1.18	1.79	2.52	2.39	1.45	1.94	1.88	0.13	0.12	0.18	0.19	0.14	0.16	0.15
Fe_2O_3(cal)	1.13	1.69	2.38	2.25	1.38	1.90	1.79	0.13	0.13	0.18	0.19	0.14	0.17	0.16
MnO	0.05	0.05	0.1	0.07	0.08	0.06	**0.07**	0.01	0.01	0.01	0.02	0.03	0.02	**0.02**
MgO	2.07	2.01	1.92	1.44	1.83	1.98	1.88	1.94	2.16	1.2	1.58	2.09	2.37	1.89
CaO	1.16	2.84	2.48	2.76	1.48	2.59	2.22	2.5	2.73	2.46	2.55	2.66	2.68	2.60
Na_2O	5.47	5.76	6.33	6.06	5.59	5.94	**5.86**	6.36	6.81	6.48	6.06	5.9	6.77	**6.40**
K_2O	0.24	0.49	0.23	0.25	0.36	0.4	0.33	0.25	0.3	0.22	0.32	0.33	0.28	0.28
LOI	0.94	1.7	1.4	1.46	0.84	0.81	1.19	0.36	0.4	0.63	0.82	1.07	0.71	0.67
Cr	2	7.39	24	15.6	3.31	5.18	**9.58**	9	15	21	17	14	15	**15.17**
Co	6.1	7.91	9.77	9.63	7.12	8.03	**8.09**	2	2	3	4.02	4.31	4.15	**3.25**
Sc	10.21	9.5	19.5	–	9.06	8.84	**11.42**	2.22	2.88	–	3.15	3.09	2.67	**2.80**
V	22	105	102	81	37	76	**70.50**	6	23	24	22.1	10.18	19.46	**17.46**
Zn	31	24	43	50	27	25	33.33	14	15	–	17	10	15	14.20
Rb	8	7	5	2.83	7	6	5.97	5	4	1.65	5	6.06	5.14	4.48
Ba	<50	<40	<70	19.7	<35	<30	–	40	115	51.1	70.36	61.34	93.07	71.81
Sr	110	133	180	174	89.34	142.18	**138.09**	227	288	456	374.66	247.51	318.44	**318.60**
Ta	0.22	0.20	0.20	0.13	0.18	0.19	**0.19**	0.15	0.15	0.06	0.12	0.11	0.1	**0.12**
Hf	2.91	2.06	2.3	3.19	3.05	2.29	2.63	2.9	3.16	3.38	3.04	2.76	3.31	3.09
Zr	35	60	95	88	71	82	71.83	39	72	117	107.14	47.86	88.61	78.60
Th	1.09	0.14	0.50	0.63	0.92	0.33	**0.60**	1.6	1.72	2.39	2.24	1.9	2.05	**1.98**
U	0.40	0.30	0.50	0.3	0.35	0.48	0.39	0.27	0.40	0.21	0.32	0.39	0.25	0.31
La	3.52	2.04	3.22	2.94	3.6	3.18	**3.08**	1.88	2.38	2.39	2.11	2.02	2.44	**2.20**
Ce	8.71	4.62	8.95	8.89	8.42	7.87	**7.91**	3.76	5.84	5.26	4.87	3.94	5.38	**4.84**
Pr	–	–	–	1.68	–	–	1.68	–	–	0.78	–	–	–	0.78
Nd	–	–	–	9.91	–	–	9.91	–	–	3.58	–	–	–	3.58
Sm	3.1	1.26	4.27	3.8	2.85	3.71	**3.17**	0.74	0.87	1.02	0.97	0.82	0.94	**0.89**
Eu	1.06	0.54	1.52	1.25	1.07	1.38	**1.14**	0.26	0.29	0.36	0.33	0.27	0.35	**0.31**
Gd	4.03	2.22	6.85	5.21	4.28	5.92	**4.75**	0.75	0.80	0.89	0.87	0.79	0.85	**0.83**
Tb	0.76	0.47	1.11	0.96	0.69	1.05	**0.84**	0.10	0.11	0.13	0.14	0.12	0.13	**0.12**
Dy	5.31	3.1	7.95	6.38	5.71	7.06	**5.92**	0.66	0.72	0.81	0.78	0.7	0.74	**0.74**
Ho	1.2	0.75	1.60	1.4	1.31	1.54	**1.30**	0.14	0.15	0.16	0.17	0.16	0.15	**0.16**
Tm	0.54	0.38	0.79	0.64	0.52	0.68	**0.59**	0.07	0.08	0.08	0.09	0.09	0.1	**0.09**
Yb	3.54	2.52	4.79	4.64	3.62	4.7	**3.97**	0.48	0.52	0.56	0.55	0.46	0.54	**0.52**
Lu	0.53	0.33	0.66	0.73	0.57	0.69	**0.59**	0.08	0.08	0.1	0.09	0.09	0.11	**0.09**
Nb	–	–	–	1	–	–	1.00	–	–	0.8	–	–	–	0.80
Y	–	–	–	40	–	–	40.00	–	–	5	–	–	–	5.00
Ga	–	–	–	18	–	–	18.00	–	–	22	–	–	–	22.00

Major elements in wt% and trace elements in ppm). $Fe_2O_3^* = Fe_2O_3$ total. Cal: calculated.

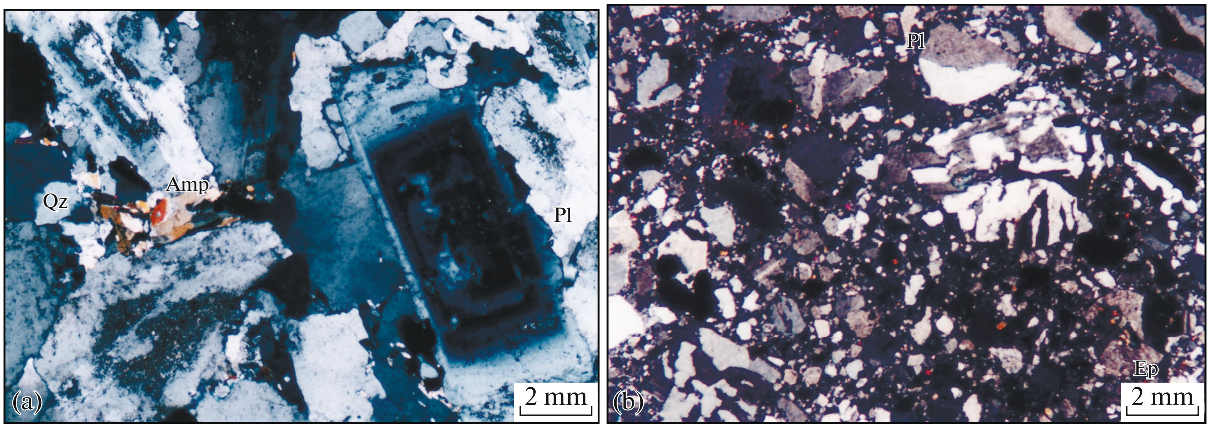

Fig. 4. Photomicrographs of the studied Cretaceous (a), and Jurassic (b) plagiogranites. Zoning of plagioclases in the Cretaceous samples (a) and graphic texture in the Jurassic ones (b) are evident.

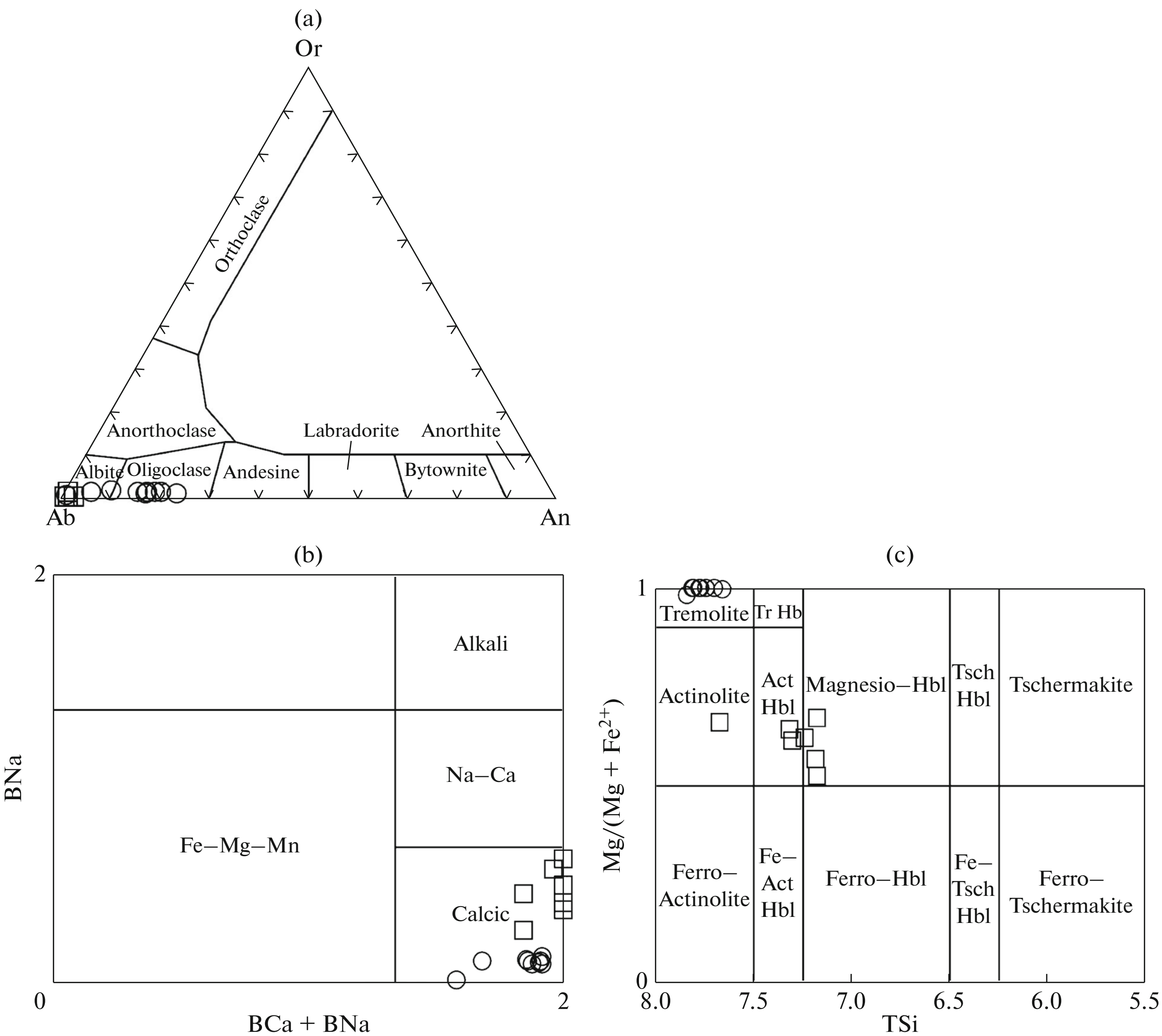

Fig. 5. Mineral chemistry diagrams of feldspars (a) [6] and amphiboles (b, c) [17] in the Ashin ophiolite plagiogranites. Circles and squares present the minerals in the Cretaceous and Jurassic samples, respectively.

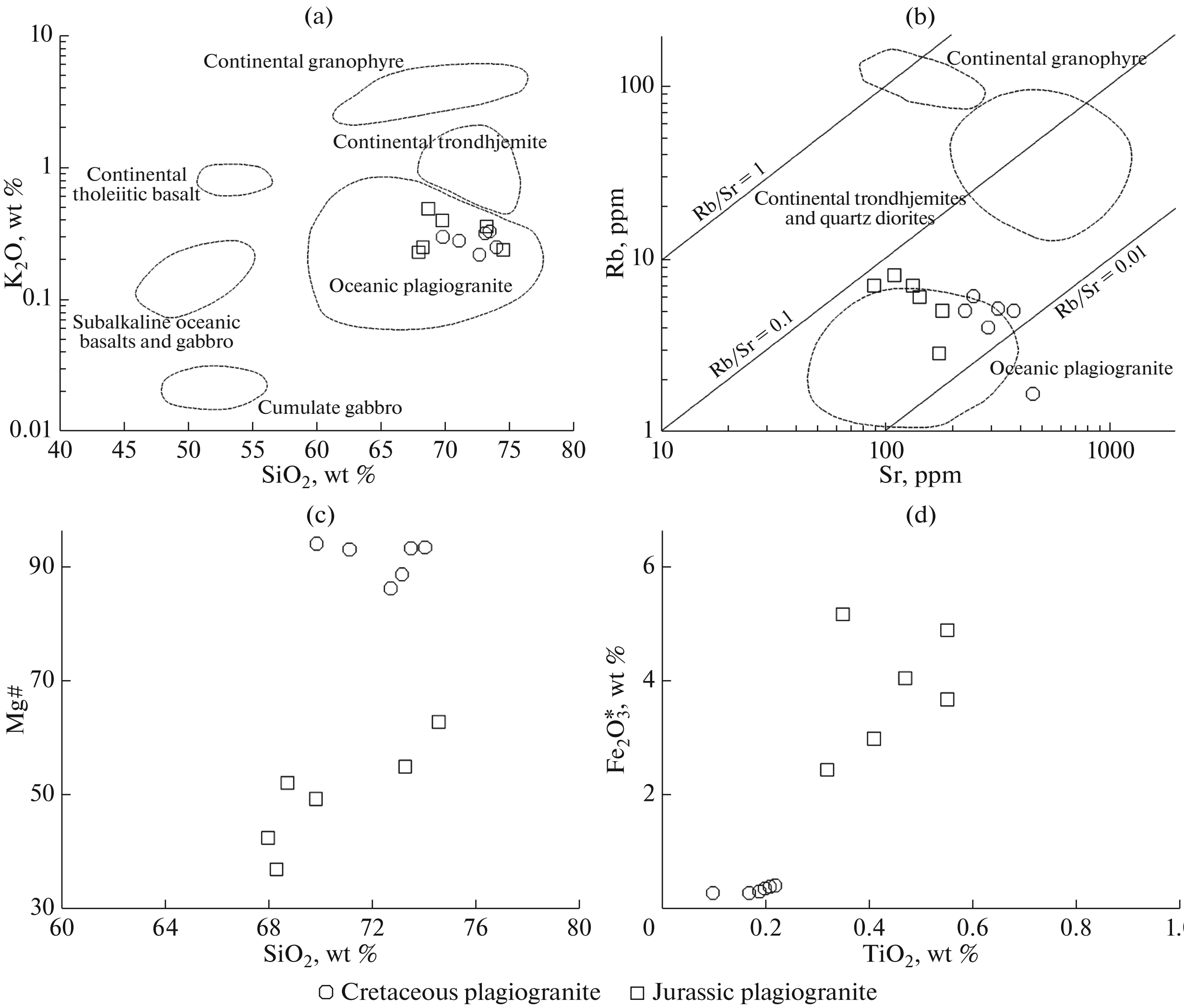

Fig. 6. (a) Semi logarithmic SiO_2 versus K_2O diagram [1, 3]; (b) Sr against Rb graph [1, 5]. These chemical diagrams indicate that the analyzed samples belong to the oceanic plagiogranite group and are different than the other acidic igneous rocks; (c, d) SiO_2–Mg# and TiO_2–$Fe_2O_3^*$ graphs indicate that the Ashin Cretaceous plagiogranites have higher Mg# and lower TiO_2 and $Fe_2O_3^*$ in comparison with the Jurassic ones.

WHOLE ROCKS GEOCHEMISTRY

Whole rock geochemical analyses of the studied plagiogranites (Table 3) shows that the SiO_2 contents of samples vary from 68.0 to 74.6 wt%, which reveal their acidic characteristic. The major (SiO_2 and K_2O) and trace (Sr and Rb) (Fig. 6) elements used to discrimination of the studied rocks from other igneous rocks show that they are similar to the oceanic plagiogranites. Low values of K_2O (0.2 to 0.4 wt%) is evident. The LOI (Loss on ignition) amounts varies from 0.8 to 1.2 wt %.

Comparison of chemical composition of the Jurassic plagiogranites with the Createaceous ones indicate that the Cretaceous samples have higher SiO_2, Al_2O_3, Na_2O, Cr, Sr, Th, and lower TiO_2, $Fe_2O_3^*$, MnO, Co, Sc, V, Ta, Nb, Y and REEs (Table 3, Fig. 6). These chemical characteristics are in agreement with higher content of amphibole in the Jurassic samples and high values of plagioclase and leucocratic nature of the Cretaceous plagiogranites.

The distinctive chemical characteristics of these two types of plagiogranite are reflected in their normative mineralogical compositions (Tables 3, 4). The Jurassic plagiogranites have higher values of hypersthene, magnetite and ilmenite (5.3, 2.6, 0.8 vol %) than the Cretaceous samples (4.1, 0.03 and 0.3 vol %), respectively.

Normative analyses of the studied samples fall in trondhjemite field of QAP diagram (along the quartz-plagioclase side, [18]) and Ab-An-Or ternary diagrams [27] (Fig. 7). The A/NK against A/CNK diagram [22]

Table 4. Calculated CIPW norm of the chemically analyzed plagiogranites from the Ashin ophiolite (Central Iran)

Sample	**Ashj11**	**Ashj12**	**Ashj13**	**Ashj14**	**Ashj15**	**Ashj16**	**Ashc21**	**Ashc22**	**Ashc23**	**Ashc24**	**Ashc25**	**Ashc26**
age	**Juras.**	**Juras.**	**Juras.**	**Juras.**	**Juras.**	**Juras.**	**Cret.**	**Cret.**	**Cret.**	**Cret.**	**Cret.**	**Cret.**
Quartz	35.86	24.33	21.70	23.74	32.99	25.21	28.46	19.97	27.51	28.85	29.61	21.84
Corundum	1.37	0.00	0.00	0.00	0.89	0.00	0.00	0.78	0.00	0.00	0.00	0.00
Zircon	0.01	0.01	0.02	0.02	0.01	0.02	0.01	0.01	0.02	0.02	0.01	0.02
Orthoclase	1.42	2.90	1.36	1.48	2.13	2.37	1.48	1.77	1.30	1.89	1.95	1.66
Albite	46.28	48.73	53.56	51.27	47.30	50.26	53.81	57.62	54.83	51.27	49.92	57.28
Anorthite	5.83	11.49	9.29	11.31	7.40	10.10	9.40	13.68	10.24	12.51	10.65	11.13
Diopside	0.00	2.13	2.53	1.98	0.00	2.26	2.42	0.00	1.67	0.23	2.06	1.80
Hypersthene	5.95	5.07	5.83	4.38	5.55	5.19	3.71	5.38	2.22	3.83	4.25	5.07
Magnetite	1.64	2.45	3.45	3.26	2.00	2.75	0.16	0.00	0.00	0.04	0.00	0.00
Hematite	0.00	0.00	0.00	0.00	0.00	0.00	0.02	0.13	0.18	0.16	0.14	0.17
Ilmenite	0.61	1.04	0.66	1.04	0.78	0.89	0.19	0.27	0.40	0.42	0.36	0.38
Rutile	0.00	0.00	0.00	0.00	0.00	0.00	0.00	0.03	0.00	0.00	0.00	0.00
Total	**98.97**	**98.16**	**98.41**	**98.50**	**99.05**	**99.04**	**99.66**	**99.65**	**98.37**	**99.23**	**98.97**	**99.34**

indicates metaluminous to slightly peraluminous characteristic of samples. Total alkalis ($Na_2O + K_2O$) versus silica diagram of [15] reveals subalkaline nature of the Ashin plagiogranites.

Trace elements values and ratios of the analyses samples [14, 28] (Fig. 8) suggest the tholeitic and calc-alkaline nature for the Jurassic and Cretaceous plagiogranites of the Ashin ophiolite, respectively.

Chondrite-normalized REE patterns of the Ashin plagiogranites (REE contents of chondrite are from [36]) indicate two distinct different patterns (Fig. 8). The Jurassic samples have higher values of REEs. In the chondrite-normalized REE patterns of the Jurassic samples (Fig. 8), the LREEs (light rare earth elements) are depleted relative to the HREEs (heavy rare earth elements) and both are enriched relative to chondrite. Some samples represent negative anomaly of Eu. One of samples (Ashj12) presents lower values of REEs than the other Jurassic samples. The Cretaceous plagiogranites are characterized by enrichment of the LREEs relative to the HREEs and a positive anomaly of Eu. The Cretaceous samples have very low values of HREEs.

Primitive mantle-normalized multi-element variation spider diagram of the Ashin ophiolite plagiogranites (normalizing values from [24]) (Fig. 8) shows positive anomalies of K and Sr, and negative anomaly of Ti. Comparison of the Ashin ophiolite plagiogranites with the Bayazeh Cretaceous continental adakite [26] in the primitive mantle-normalized spider diagram reveal higher LILE (large ion lithophile elements) (e.g., Cs, Rb, Ba, Sr, and K) and LREEs and lower HREEs of the continental adakites.

DISCUSSION

Petrogenesis

The petrogenesis of ophiolitic plagiogranites can be attributed to the various magmatic and hydrothermal processes. Several processes have been suggested and discussed to explain the plagiogranite genesis in ophiolites (eg. [2, 4, 8, 16, 21, 42]): 1—extremely fractional crystallization of a low-K tholeitic MORB magma at low pressures; 2—partial melting of hydrated mafic rocks of oceanic crust (eg. metabasalt and amphibolite); 3—liquid immiscibility in silicates melts; and 4—assimilation and partial melting of highly hydrothermally altered basic sheeted dykes in fast spreading ridges. Our subsequent discussions reveal that the first two processes play important role in formation of plagiogranites in the studied ophiolite.

Comparison of the major elements values and chondrite-normalized REE patterns (Fig. 8), as well as the primitive mantle-normalized multi-elements spidergrams of the Jurassic and Cretaceous plagiogranites of the Ashin ophiolite reveal that they are distinctly different from each other, which points to their different origin.

The negative Eu anomaly in the chondrite-normalized REE patterns of the Jurassic plagiogranites can be attributed to the early abtraction of Eu from the primary basaltic melt by crystallization and removal of calcic plagioclase. Positive anomalies of Eu in mafic cumulate gabbros associated with plagiogranites of ophiolites, and similar portioning of Eu between cumulus phases and residual magma [4] support this hypothesis. According to this, the Ashin Jurassic plagiogranites are late-stage differentiate of a quartz-normative basaltic magma. These plagiogranites are end members of the differentiation products of the ophiol-

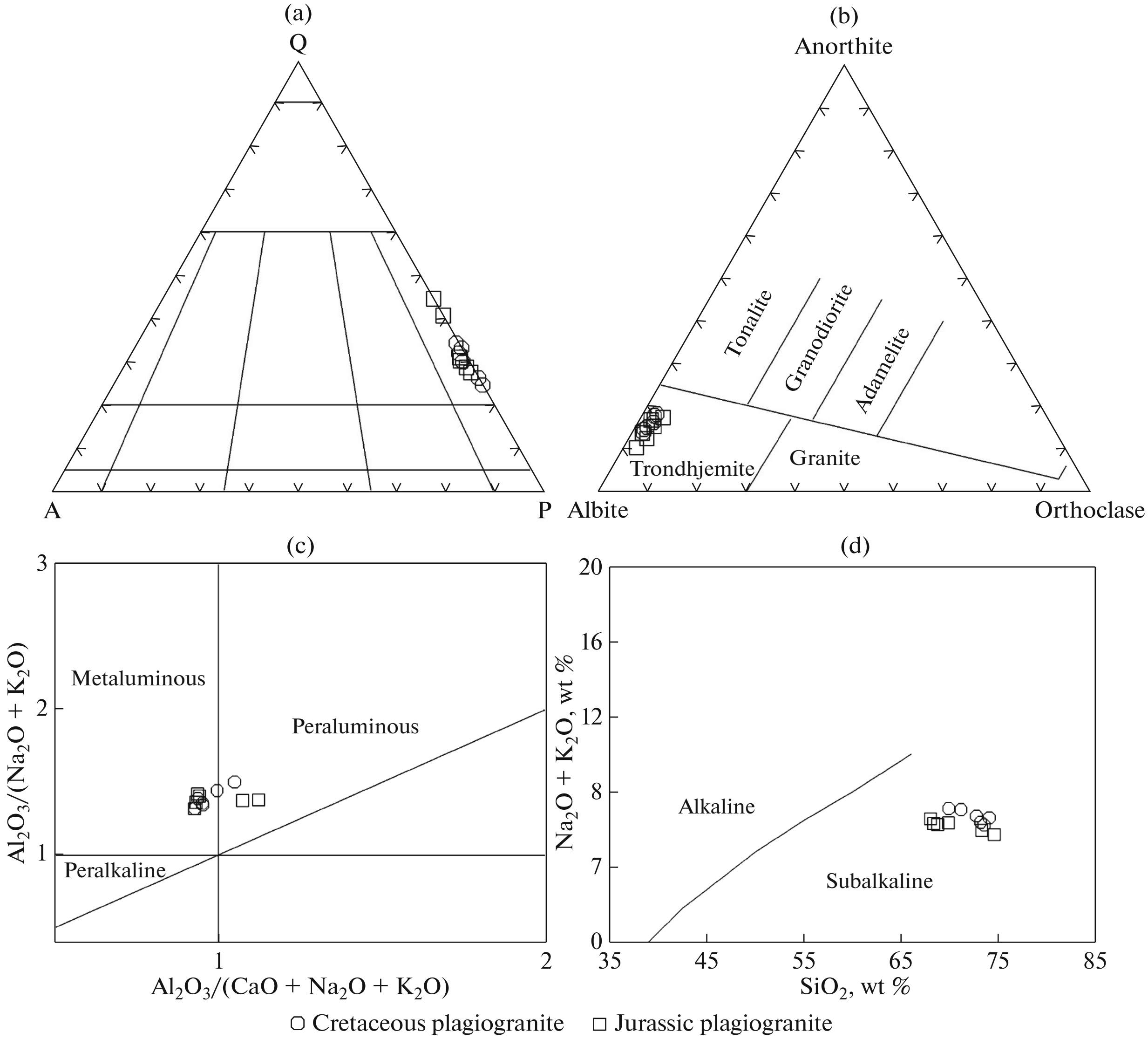

Fig. 7. Normative and major elements geochemical diagrams of the Ashin ophiolite plagiogranites. (a) Quartz–Alkali-feldspar–Plagioclase (QAP) normative-based classification scheme [18]. All samples plotted on the right side of the QAP triangle; in the field of trondhjemite; (b) Normative Albite–Anorthite–Orthoclase ternary diagram [27] proposes the trondhjemite term; (c) The A/NK versus A/CNK diagram shows metaluminous to slightly peraluminous characteristic of samples [22]; (d) SiO_2 against ($Na_2O + K_2O$) graph [15] reveals subalkaline nature of the studied plagiogranites.

itic suite. The negative Eu anomaly in the plagiogranites support the fractional crystallization model in their petrogenesis [20]. Fractional crystallization of 70–85% of clinopyroxene + feldspar ± amphibole of a gabbroic source material can generate acid plagiogranitic melts [11, 21]. The SiO_2 and TiO_2 contents (68–75 and 0.3–0.6 wt %, respectively) of the Jurassic plagiogranites confirm that they are formed by MORB differentiation [16].

Positive anomaly of Eu in the Cretaceous samples suggests that plagioclase accumulation played important role in magmatic evolution. Leucocratic nature and low values of MgO, $Fe_2O_3^*$, MnO, Co, Sc, V and HREEs in the Ashin Cretaceous plagiogranites indicate that they are formed by partial melting of a mafic rock [7, 9, 10] and a peridotite can not be the source rock of the Cretaceous samples. Petrogenetic calculations indicate that 5–15% partial melting of supra subduction zone (SSZ) gabbros and amphibolites can generate plagiogranitic melts with SiO_2 ranging from ~67 to 80 wt % [11, 19, 21, 31]. The SiO_2 values of (70–74 wt %) and low TiO_2 contents (0.1–0.2 wt %) of the Cretaceous plagiogranites from Ashin ophiolite indicate that they are products of partial melting of amphibolites and gabbros in a SSZ setting [16]. Dehydration melting of amphibolites is discussed in some researches as [44, 45].

The all above field, petrography, geochronological and geochemical characteristics indicate two distinct

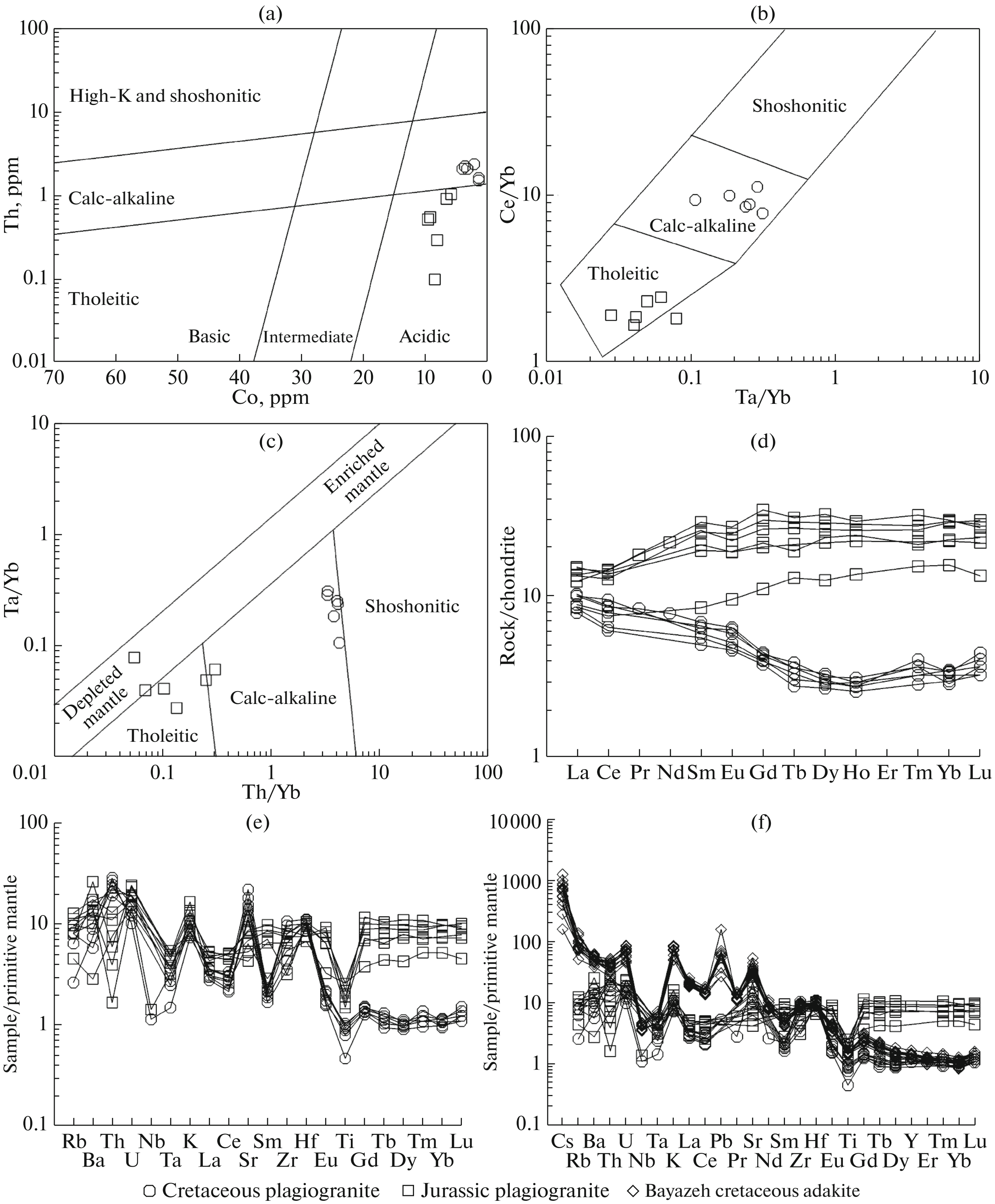

Fig. 8. (a) Co versus Th graph [14]; (b) Ta/Yb against Ce/Yb and (c) Th/Yb versus Ta/Yb diagrams [28]. These trace element geochemical plots suggest tholeitic and calc-alkaline nature for the Jurassic and Cretaceous plagiogranites of the Ashin ophiolite, respectively. (d) Chondrite-normalized REE patterns of the analyzed samples. The REE contents of chondrite are taken from [36]; (e) Primitive mantle-normalized multi-element spider diagram. Normalizing values are from [24]. (f) Comparison of the Ashin ophiolite plagiogranites with the Bayazeh Cretaceous continental adakites [26] in the primitive mantle-normalized variation diagram.

suites of plagiogranites within the Ashin ophiolitic melange. They represent mid ocean spreading and subduction-related settings, for the Jurassic and Cretaceous plagiogranites, respectively. The younger plagiogranites were likely derived from the anatexis of amphibolites, in an intra-oceanic back arc basin.

Geodynamic Significance Inferred from Geochemical Data

Tholeitic nature, higher HFSE (Ti, Nb, Ta) and lower LILE (Sr, Ba, Th) contents in the Jurassic plagiogranites points to the mid-ocean ridge origin. About of the Cretaceous samples, these chemical characteristics (calc-alkaline nature, low HFSE and high LILE) support their subduction-related origin. The slightly enriched patterns of the LREEs in the studied Cretaceous plagiogranites; as well as the negative anomalies of Ti, Nb and Ta; and low concentrations of HREEs indicate that they were likely derived from the partial melting of an amphibolite in a subduction zone [7, 12, 31]. Therefore, the Ashin Jurassic and Cretaceous plagiogranites are similar to the plagiogranites of the normal ocean ridges and the suprasubduction zone plagiogranites [28], respectively.

Regional geology and petrological studies show that the Ashin ophiolite has passed two period of activity with production of dikes, pillow lavas and plagiogranites in lower Jurassic and Upper Cretaceous [35]. In the Middle Jurassic, Ashin ophiolite suffered a metamorphism in amphibolite facies P–T condition that possibly relates to the first closure of the Ashin oceanic crust. Metamorphic rocks of Ashin ophiolite have produced through this metamorphic episode. The final closure of this oceanic crust and obduction has occurred in Paleocene to Eocene. Nearly the same geological history of two various magmatic phases in an ophiolite is reported by Shirdashtzadeh et al. [34] about of Naein (Nain) ophiolite, which is situated at the south of the Ashin ophiolite (Fig. 1). In the Naein ophiolite, two Early Jurassic and Cretaceous magmatic phases recognized. Jurassic rocks of the Naein ophiolite are possibly metamorphosed in the amphibolite facies P–T condition in the Middle Cimmerian orogenic episode.

Comparison of chemical composition of Jurassic and Cretaceous plagiogranites of the Ashin ophiolite indicate that tectonic setting of the Ashin ophiolite has changed from a normal mid-ocean ridge setting in the Jurassic to a supra-subduction (back-arc) setting in the Cretaceous. This study shows the appearance of two Mid-ocean ridge type (MOR-type) and suprasubduction zone (SSZ) type ophiolitic rocks with clearly different ages in a single ophiolite massive.

All plagiogranites of the Ashin ophiolite have lower values of LILE and LREE than the Cretaceous continental adakites of Central Iran (Fig. 8f). But the HREE contents of Cretaceous plagiogranites are similar to the Cretaceous continental adakites, which possibly point to the same non-peridotitic source rock of them. They are possibly have formed by partial melting of an amphibolitic source rock in a subducting oceanic crust. The Cretaceous plagiogranites of the Ashin ophiolite are oceanic adakites and have lower values of LILE than the continental ones (Fig. 8f). This type of Ashin plagiogranites are formed by partial melting of hydrated basic rocks in a subducted oceanic crust. Geochemical criteria of this type of plagiogranite is consistent with partial melting of subducted oceanic crust during the collision and subduction of an active spreading center [33]. The calc-alkaline trend and mechanism of formation of Cretaceous plagiogranites resemble as adakites reported from other Iranian ophiolites [37]. These acidic melts which are formed by partial melting of basic rocks in the subducted oceanic slab, should pass through the overlying mantle wedge and react with the wall rock peridotites during their ascent [23]. The low and variable content of Cr (9–21 ppm; Ave.:15 ppm) in the Cretaceous plagiogranites reveal limited degrees of interaction with peridotites and a thin mantle wedge over the slab melting zone. The Cr content of Cretaceous plagiogranites Cr (9–21 ppm; Ave.:15 ppm) is higher than its values in the Jurassic ones (2–16 ppm; Ave.:10 ppm).

CONCLUSIONS

Regional geology and petrological studies of plagiogranites in the Ashin Mesozoic ophiolite suggest that two different types of plagiogranites have been formed in Jurassic and Cretaceous of this ophiolite. These two types of plagiogranites are formed in different ways and at different geological eras. The older one may possibly formed by progressive fractional crystallization of a MORB- type magma produced by partial melting of mantle peridotites in a normal ridge-related tectonic setting. On the other hand, the Cretaceous plagiogranites present the petrological and geochemical criteria of formation in a subduction-related tectonic setting. This study reveals change in tectonic setting of the Ashin ophiolite oceanic crust through the Mesozoic from a normal mid-ocean ridge to a suprasubduction zone.

ACKNOWLEDGMENTS

The authors thank the University of Isfahan (Iran) and Kanazawa University (Japan) for financial support. This paper has greatly benefited from the helpful and constructive comments by reviewers Prof. Dr. Marina V. Luchitskaya and Prof. Dr. Andrey A. Shchipansky.

REFERENCES

1. F. Barker, "Trondhjemite: Definition, environment and hypotheses of origin," in *Trondhjemites, Dacites*

and Related Rocks, Ed. by F. Barker (Elsevier, Amsterdam, 1979), pp.1–12.

2. J. S. Beard and G. E. Lofgren, "Dehydration melting and water-saturated melting of basaltic and andesitic greenstones and amphibolites at 1, 3, and 6.9 kb," J. Petrol. **32**, 365–401 (1991).
3. R. G. Coleman, *Ophiolites – Ancient Lithosphere?* (Springer, New York, 1977).
4. R. G. Coleman and M. M. Donato, "Oceanic plagiogranite revisited," in *Trondhjemites, Dacites and Related Rocks,* Ed. By F. Barker (Elsevier, Amsterdam, Netherlands, 1979), pp. 149–168.
5. R. G. Coleman and Z. E. Peterman, "Oceanic plagiogranite," J. Geophys. Res. **80**, 1099–1108 (1975).
6. W. A. Deer, R. A. Howie, and J. Zussman, *An Introduction to the Rock-Forming Minerals* (Longman, London, 1991).
7. M. J. Defant and M. S. Drummond, "Derivation of some modern arc magmas by melting of young subducted lithosphere," Nature **347**, 662–665 (1990).
8. S. Dixon and M. J. Rutherford, "Plagiogranites as late stage immiscible liquids in ophiolite and mid-ocean ridge suites: An experimental study," Earth Planet. Sci. Lett. **45**, 45–60 (1979).
9. M. S. Drummond and M. J. Defant, "A model for trondhjemite-tonalite-dacite genesis and crustal growth via slab melting: Archean to modern comparisons," J. Geophys. Res., [Solid Earth Planets] **95**, 21503–21521 (1990).
10. M. S. Drummond, M. J. Defant, and P. K. Kepezhinskas, "Petrogenesis of slab-derived trondhjemite–tonalite–dacite/adakite magmas," Trans. R. Soc. Edinburgh: Earth Sci. **87**, 205–215 (1996).
11. P. A. Floyd, M. K. Yaliniz, and M. C. Goncuoglu, "Geochemistry and petrogenesis of intrusive and extrusive ophiolitic plagiogranites, Central Anatolian Crystalline Complex, Turkey," Lithos **42**, 225–241 (1998).
12. S. Foley, M. Tiepolo, and R. Vannucci, "Growth of early continental crust controlled by melting of amphibolite in subduction zones," Nature **417**, 837–840 (2002).
13. C. B. Grimes, T. Ushikubo, R. Kozdon, and J. W. Valley, "Perspectives on the origin of plagiogranite in ophiolites from oxygen isotopes in zircon," Lithos **179**, 48–66 (2013).
14. A. R. Hastie, A. C. Kerr, J. A. Pearce, and S. F. Mitchell, "Classification of altered volcanic island rocks using immobile trace elements, development of the Th–Co discrimination diagram," J. Petrol. **48**, 2341–2357 (2007).
15. T. N. Irvine and W. R. A. Baragar, "A guide to the chemical classification of the common volcanic rocks," Can. J. Earth Sci. **8**, 523–548 (1971).
16. J. Koepke, J. Berndt, S. T. Feig, and F. Holtz, "The formation of SiO_2-rich melts within the deep oceanic crust by hydrous partial melting of gabbros," Contrib. Mineral. Petrol. **153**, 67–84 (2007).
17. B. E. Leake, A. R. Woolley, C. E. S. Arps, W. D. Birch, M. C. Gilbert, J. D. Grice, F. C. Hawthorne, A. Kato, H. J. Kisch, V. G. Krivovichec, K. Linthout, J. Laird, J. Mandarino, W. V. Maresch, E. H. Nickel, et al., "Nomenclature of amphiboles; Report of the Subcommittee on amphiboles of the International Mineralogical Association Commission on New Minerals and Mineral Names," Eur. J. Mineral. **9**, 623–651 (1997).
18. R. W. Le Maitre, *Igneous Rocks: A Classification and Glossary of Terms*, 2nd ed., (Cambridge Univ. Press, Cambridge, 2002).
19. M. V. Luchitskaya, O. L. Morozov, and S. A. Palandzhyan, "Plagiogranite magmatism in the Mesozoic island-arc structure of the Pekulney Ridge, Chukotka Peninsula, NE Russia," Lithos **79**, 251–269 (2005).
20. M. V. Luchitskaya, "Plagiogranites of the Kuyul ophiolite massif (northeastern Kamchatka, Koryak Upland)," Ofioliti **21**, 131–138 (1996).
21. A. Magganas, "Plagiogranitic rocks of Evros Ophiolite, NE Greece," Bull. Geol. Soc. Greece, **40**, 884–898 (2007).
22. P. D. Maniar and P. M. Piccoli, "Tectonic discrimination of granitoids," Bull. Geol. Soc. Am. **101**, 635–643 (1989).
23. H. Martin, R. H. Smithies, R. Rapp, J. F. Moyen, and D. Champion, "An overview of adakite, tonalite-trondhjemite-granodiorite (TTG), and sanukitoid: Relationships and some implications for crustal evolution," Lithos **79**, 1–24 (2005).
24. W. F. McDonough and S. S. Sun, "The composition of the Earth," Chem. Geol. **120**, 223–253 (1995).
25. E. A. K. Middlemost, "Iron oxidation ratios, norms and the classification of volcanic rocks," Chem. Geol. **77**, 19–26 (1989).
26. N. Nosouhian, G. Torabi, and S. Arai, "Late Cretaceous dacitic dyke swarm from Central Iran, a trace for amphibolite melting in a subduction zone," Geotectonics **50**, 295–312 (2016).
27. J. T. O'Connor, "A classification for quartz-rich igneous rock based upon feldspar ratios," in *Geological Survey Research 1965, Chapter B*, Vol. 525B of *U.S. Geol. Surv., Prof. Pap.* (U.S. Gov. Print Office, Washington, DC, 1965), pp. B79–B84.
28. J. A. Pearce, N. B. W. Harris, and A. G. Tindle, "Trace element discrimination diagrams for the tectonic interpretation of granitic rocks," J. Petrol. **25**, 956–983 (1984).
29. H. R. Rollinson, "Ophiolitic trondhjemites: an analogue for the formation of Hadean felsic 'crust'," Terra Nova **20**, 364–369 (2008).
30. H. R. Rollinson, "New models for the genesis of plagiogranites in the Oman ophiolite," Lithos **112**, 603–614 (2009).
31. T. Rushmer, "Partial melting of two amphibolites: Contrasting experimental results under fluid-absent conditions," Contrib. Mineral. Petrol. **107,** 41–59 (1991).
32. M. Sharkovski, M. Susov, B. Krivyakin, L. Morozov, V. Kiristaev, and E. Romanko, *Geology of the Anarak area (Central Iran): Report TE/No.19* (Geol. Surv. Iran, 1984).
33. J. W. Shervais, "Tonalites, trondhjemites, and diorites of the Elder Creek ophiolite, California: Low-pressure slab melting and reaction with the mantle wedge," in *Ophiolites, Arcs, and Batholiths: A Tribute to Cliff Hopson*, Vol. 438 of *Geol. Soc. Am., Spec. Pap.*, Ed. by J. E. Wright and J. W. Shervais (2008), pp. 113–132.

34. N. Shirdashtzadeh, G. Torabi, and S. Arai, "Metamorphism and metasomatism in the Jurassic Nain ophiolithic mélange, Central Iran," Neues Jahrb. Geol. Palaeontol., Abh. **255**, 255–275 (2009).

35. N. Shirdashtzadeh, G. Torabi, and S. Arai, "Two Mesozoic oceanic phases recorded in the basic and metabasic rocks of the Nain and Ashin-Zavar ophiolitic mélanges (Isfahan province, Central Iran)," Ofioliti **36**, 191–205 (2011).

36. S. S. Sun and W. F. McDonough, "Chemical and isotopic systematics of oceanic basalts: implications for mantle composition and processes," in *Magmatism in Ocean Basins*, Vol. 42 of *Geol. Soc. London, Spec. Publ.*, Ed. by A. D. Saunders and M. J. Norry, (1989), pp. 313–346.

37. G. Torabi, "Late Permian post-ophiolitic trondhjemites from Central Iran: a mark of subduction role in growth of Paleozoic continental crust," Island Arc **21**, 215–229 (2012).

38. G. Torabi, "Middle Eocene volcanic shoshonites from western margin of Central-East Iranian Microcontinent (CEIM), a mark of previously subducted CEIM-confining oceanic crust," Petrology **19**, 675–689 (2011).

39. G. Torabi, "Early Oligocene alkaline lamprophyric dykes from the Jandaq area (Isfahan Province, Central Iran): An evidence of CEIM confining oceanic crust subduction," Island Arc **19**, 277–292 (2010).

40. G. Torabi, S. Arai, and H. Abbasi, "Eocene continental dyke swarm from Central Iran (Khur area)," Petrology **22**, 1–16 (2014).

41. G. Torabi, N. Shirdashtzadeh, S. Arai, and J. Koepke, "Paleozoic and Mesozoic ophiolites of Central Iran: Amphibolites from Jandaq, Posht-e-Badam, Nain and Ashin ophiolites," Neues Jahrb. Geol. Palaeontol., Abh. **262**, 227–240 (2011).

42. T. Üner, Ç. Üner, Y. Özdemir, and R. Arat, "Geochemistry and origin of plagiogranites from the Eldivan Ophiolite, Çankırı (Central Anatolia, Turkey)," Geol. Carpathica **65**, 195–205 (2014).

43. D. L. Whitney and B. W. Evans, "Abbreviations for names of rock-forming minerals," Am. Mineral. **95**, 185–187 (2010).

44. P. J. Wyllie and M. B. Wolf, "Amphibolite-dehydration melting: sorting out the solidus," in *Magmatic Processes and Plate Tectonics*, Vol. 76 of *Geol. Soc. London, Spec. Publ.*, Ed. by Ed. by H. M. Pritchard, T. Alabaster, N. B. W. Harris, and C. R. Neary (London, 1993), pp. 405–416.

45. M. B. Wolf and P. J. Wyllie, "Dehydration-melting of amphibolite at 10 kbar: Effects of temperature and time," Contrib. Mineral. Petrol. **115**, 369–383 (1994).

Reviewers: M.V. Luchitskaya and A.A. Shchipansky